frontiers | Frontiers in Energy Research

TYPE Original Research
PUBLISHED 20 August 2024
DOI 10.3389/fenrg.2024.1437271

OPEN ACCESS

EDITED BY
Yu Huang,
Nanjing University of Posts and Telecommunications, China

REVIEWED BY
Dardan Klimenta,
University of Pristina, Serbia
Omid Shariati,
University of Reading, United Kingdom

*CORRESPONDENCE
Zhou Zidong,
zzd774570699@163.com

RECEIVED 23 May 2024
ACCEPTED 24 July 2024
PUBLISHED 20 August 2024

CITATION
Zidong Z and Jinquan Z (2024) Security-constrained unit commitment model considering frequency and voltage stabilities with multiresource participation.
Front. Energy Res. 12:1437271.
doi: 10.3389/fenrg.2024.1437271

Security-constrained unit commitment model considering frequency and voltage stabilities with multiresource participation

Zhou Zidong* and Zhao Jinquan

College of Electrical Engineering, Shanghai University of Electric Power, Shanghai, China

The rapidly increasing proportion of renewable energy sources has led to a reduction in the relative share of synchronous units, which has resulted in a decline in the inertia of the power system and a decrease in its voltage support capacity. This has led to several issues related to the frequency and voltage stabilities of the power system. To ensure these frequency and voltage stabilities, it is necessary to maintain a number of synchronous units online in the day-ahead generation schedule. First, the dynamic frequency change process after a power system fault is discussed, and a linear expression is derived for the frequency stability constraints involving energy storage systems and wind turbines. Second, the short-circuit capacity of the bus is characterized to describe the strength of voltage support, and the minimum short-circuit capacity requirement of the bus is solved based on the transient voltage recovery problem after clearance of the short-circuit faults. The total short-circuit capacity provided by the unit to the bus is then calculated through the network reactance matrix to establish the voltage stability constraint. Subsequently, the security-constrained unit commitment model considering frequency and voltage stabilities (FVS-SCUC) is established. Finally, the effectiveness of the proposed model is demonstrated through a numerical simulation of the IEEE-39 system comprising storage and wind turbines. The model ensures the frequency and voltage securities of the system, and the renewable energy output is improved upon considering energy storage. Thus, the overall system cost was reduced by nearly 30% by considering the frequency regulation effects of the energy storage system and wind turbine as well as the voltage regulation effects of the energy storage system.

KEYWORDS

energy storage, frequency stability, network reactance matrix, security-constrained unit commitment, voltage stability, wind turbine

Abbreviations: FSC, frequency stability constraint; VSC, voltage stability constraint; FVS-SCUC, security-constrained unit commitment model considering frequency and voltage stabilities; PFR, primary frequency regulation; PWL, piecewise linearization; VSG, virtual synchronous generator; RoCoF, rate of change of frequency; SoC, state of charge; UC, unit commitment.

1 Introduction

Ensuring the security and economic operations of power systems over extended periods of time is a primary objective of their development (Xia et al., 2013). Given the widespread integration of energy storage systems and wind turbines, the proportion of synchronous units within the power system has decreased gradually, which has severely weakened the inertial and voltage support capabilities of the system under the same active disturbances (Lin et al., 2023a). Currently, the frequency-constrained unit commitment (FCUC) model that considers frequency stability has received widespread attention, where the inertia of the power system serves as a widely employed pivotal indicator to assess the frequency support capability. Zhang et al. (2021) defined and modeled the inertia of various resources within the power system, and their study delved into the effects of inertia on system stability and mechanisms of the power angle. Furthermore, they consolidated the evaluation methods for power system inertia. Subsequently, the FCUC model accompanied by various linearization approaches was proposed for the frequency nadir constraint. Teng et al. (2016) linearized the minimum frequency constraint post-fault by simplifying the dynamic frequency response characteristics; however, the process of deriving the minimum frequency constraint involves a logarithmic function that poses challenges for swift resolution. Badesa et al. (2019) introduced a linearization method to address this non-linear constraint, where binary variables are used to represent the primary frequency regulation power provided by the units.

Zhang et al. (2020) utilized the frequency safety margin to analyze the impact of renewable energy injection on frequency stability. Badesa et al. (2021a,2021b) evaluated the frequency characteristics of the diverse regions within the system and established a linear model depicting the variation characteristics of the inertial center frequency. Yang et al. (2022) proposed employing the time-domain integration of the frequency deviation during the primary and secondary frequency regulation processes as an indicator to assess the frequency stability and established a two-stage stochastic FCUC model. Wang et al. (2020) proposed a security-constrained unit commitment (SCUC) model by considering the dynamic frequency with post-disturbance frequency nadir as the characteristic constraint and used Benders decomposition for the two-stage solution. Li et al. (2023a) proposed a market mechanism for the inertia and primary frequency response as well as an enhanced piecewise linearization (PWL) method to establish a linear expression for the frequency nadir constraint to facilitate model solving. Tuo and Li (2023) explored the impacts of the system region oscillations on the initial maximum rate of change of frequency (RoCoF) and used the PWL technique to linearize the RoCoF constraint.

Given the significant roles of storage systems in enhancing the frequency stabilities of renewable energy systems (Wang et al., 2022) and their potential to mitigate wind turbine curtailment when integrated at the grid connection buses (Zheng et al., 2014), numerous scholars have integrated storage into the frequency stability constraints (FSCs). Among these scholars, Zhu et al. (2024) examined the influences of the synchronous units, storage inertia, and primary frequency regulation (PFR) on frequency stability within the SCUC model, while Xu et al. (2020) analyzed the low inertia characteristics of energy storage on frequency stability. These works predominantly focus on the study of SCUC with an emphasis on frequency stability. Traditional SCUC models rely on linear network security constraints based on DC power flow, whereas the voltage stability analyses typically employ non-linear AC power flow models. Consequently, constructing simple and linear voltage stability constraints (VSCs) in the SCUC models poses a significant challenge.

Presently, the prevalent approach among scholars is to construct voltage stability assessments based on indicators, such as short-circuit ratio and short-circuit capacity. Yu et al. (2022a) introduced a short-circuit ratio index to evaluate the voltage support capacity and proposed independent analyses of the frequency and voltage support strengths within the system. Similarly, Fu et al. (2024) proposed a transient overvoltage risk assessment method for multiple renewable short-circuit ratio (MRSCR) at renewable energy stations; this method analyzes the correlation between the MRSCR and transient overvoltage at the grid connection buses, in addition to identifying the key influencing factors to conduct the risk assessments accordingly. Yu et al. (2022b) considered the short-circuit ratio indexes of renewable-energy grid-connected systems and proposed a method for calculating the critical short-circuit ratio to evaluate the voltage support strength. Sun et al. (2023) considered the interplay between multiple feeding branches in renewable-energy grid-connected systems; they established a mathematical model to analyze the transient overvoltage in a single-feeding system to determine its minimum short-circuit capacity and maximum reactive power scale. Regarding the specific characteristics of wind turbines, Wu et al. (2022) assessed the applicability of the short-circuit ratio index to various issues in wind-power grid-connected systems, including static voltage stability, transient voltage stability, and sub/ultra-synchronous oscillations; they showed that enhancing the short-circuit ratio index effectively bolstered the stability of the system.

Researchers have also explored transient voltage stability considerations and proposed some assessment criteria. Xue et al. (1999) introduced some evaluation methodologies and metrics for transient voltage stability by delineating it under two categories: voltage stability and voltage drop acceptable range; they then proposed quantitative indicators to assess the transient voltage stability and voltage drop. Li et al. (2023b) studied the mechanisms of transient voltage instability within single-unit and load systems; they demonstrated the consistency between critical points in the static P-V and V-Q curves of a given system as well as proposed some calculation methods and stability criteria for the quantitative indicators of transient voltage stability.

Meanwhile, Niu et al. (2021) advocated the use of the short-circuit current weight index as a weighting factor to supply short-circuit capacity to the system; they established a quantitative relationship between the short-circuit capacities of conventional units and each of the bus bars by integrating the short-circuit capacity constraints into the SCUC model. Jiang et al. (2021) proposed a unit commitment (UC) model incorporating transient VSCs; this model delineates the linear stability cut constraints via time-domain simulation trajectory sensitivity analysis and embeds them in the UC model.

Lin et al. (2023b) proposed the necessity of meeting the short-circuit capacity requirements and transient voltage support

TABLE 1 Summary of references.

Method	First-order rotor motion equation based on the frequency dynamic response characteristics	Time-domain integration of the frequency disturbance trajectory after a fault	Benders cuts to handle the frequency stability constraint subproblems	Piecewise linearization technique to handle the frequency stability constraints
Frequency stability	Zhang et al. (2021), Teng et al. (2016), Badesa et al. (2019), Zhang et al. (2020)	Badesa et al. (2021a), Badesa et al. (2021b), Yang et al. (2022)	Wang et al. (2020)	Li et al. (2023a), Tuo and Li (2023)
Method	Short-circuit ratio index	Transient voltage stability evaluation indicators	Convert non-linear constraints to linear constraints	—
Voltage stability	Yu et al. (2022a), Fu et al. (2024), Yu et al. (2022b), Sun et al. (2023), Wu et al., (2022)	Xue et al. (1999), Li et al. (2023b), Niu et al. (2021), Jiang et al. (2021); Lin et al. (2023b)	Zhongda and Fei (2023)	—
Considered energy storage	Wang et al. (2022), Zheng et al. (2014), Zhu et al. (2024a), Xu et al. (2020)			

capabilities by employing the MRSCR to construct the VSCs. Furthermore, Zhongda and Fei (2023) effectively transformed the non-linear static VSC into the second-order cone format to achieve an overall mixed-integer second-order cone form by drawing from AC power flow principles to derive the VSC. The SCUC model proposed in this study considers both frequency stability and static voltage stability by recognizing the significant influences of synchronous units and inverter-based generators. The aforementioned studies summarize the main contributions of previous scholars, and the summary of references is shown in Table 1.

Based on the above review, the severity of frequency and voltage stability challenges within renewable energy power systems should be acknowledged, and the substantial impacts of storage and renewable energy integration should be considered. Thus, the main contributions of this study are as follows:

1. The SCUC model considering frequency and voltage stabilities (FVS-SCUC) is proposed, and its effectiveness is verified through the IEEE-39 system with integrated storage and wind turbines.
2. The impacts of storage and wind turbines on frequency stability are considered along with the short-circuit capacity provided by the storage to the buses; thus, the proposed SCUC model also considers storage and wind turbines, and its effectiveness is verified.

2 FSC with multiresource participation

2.1 Equivalent single-unit and single-load system

In the single-unit and single-load system comprising the synchronous generator, energy storage, wind turbine inertia response, and primary frequency regulation, the dynamic response of the frequency can be described by the first-order ordinary differential equation:

$$\frac{2H_{system}(t)}{f_0}\cdot\frac{df(t)}{dt}=\sum_{i=1}^{N_g}P_{g,i}^{PFR}+\sum_{i=1}^{N_s}P_{e,i}^{PFR}+\sum_{i=1}^{N_w}P_{w,i}^{PFR}-P_{loss}, \quad (1)$$

where $H_{system}(t)$ is the inertia of the power system at time t; f_0 denotes the nominal frequency level; $df(t)$ is the frequency deviation at fault occurrence at time t during the day; $P_{g,i}^{PFR}$, $P_{e,i}^{PFR}$, and $P_{w,i}^{PFR}$ are the primary frequency regulation power increments by the thermal unit, energy storage, and wind turbine; N_g, N_s, and N_w are the numbers of thermal units, energy storage systems, and wind turbines; P_{loss} is the total power deficit.

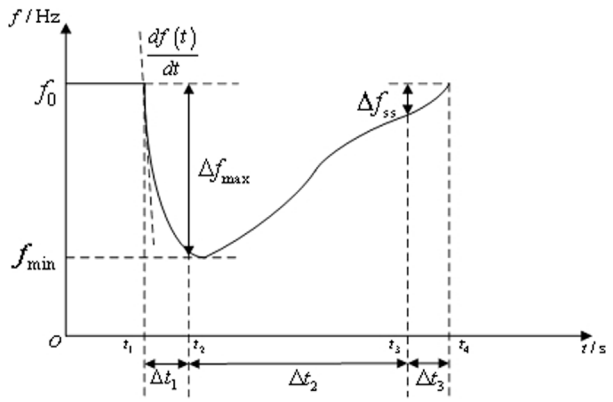

FIGURE 1
Frequency dynamic response characteristic curve of the power system.

2.2 Dynamic frequency response characteristics of the power system

The dynamic frequency response characteristic of a power system following an active power disturbance is as shown in Figure 1; this is based on the assumption that the power disturbance in the system occurs at the initial moment t_1 while the load is increasing. Trovato et al. (2019) summarized the frequency dynamic response of the system by dividing it into three stages as Δt_1, Δt_2, and Δt_3. Here, the first stage Δt_1 is the inertial response where the rotors of each synchronous unit in the system provide inertial support to suppress the frequency changes as characteristics of the rotors themselves; the second stage Δt_2 is the primary frequency modulation step where each synchronous unit in the system relies on a speed controller to increase its active power and suppress the frequency drops, even as frequency deviations

exist; the third stage Δt_3 is the secondary frequency modulation step where the frequency regulators of some units are involved in increasing the active power and restoring the frequency to normal values. The characteristics that describe the frequency changes mainly include the initial RoCoF $df(t)/dt$, maximum frequency deviation $\Delta f_{\max}$, and quasi-steady-state frequency deviation Δf_{ss}.

The power disturbances mainly refer to the active power deficits caused by emergency accidents, such as a sudden increase in the load and a generator outage. In the dynamic frequency response model of the PFR of the power system, the frequency modulation effects of the load are ignored, and the FSCs are derived as noted below.

2.3 RoCoF constraint with multiresource participation

The virtual inertia and primary frequency response are achieved through conservation of a portion of the capacity in the networked energy storage. In contrast to conventional units, the inertial constants of the energy storage systems are achieved through control strategies (analogous to those employed in wind and photovoltaic power systems).

The virtual mechanical time constant of storage i is represented as

$$0 \le T_{e,i,t} \le T_{e,i,\max},$$

where $T_{e,i,t}$ is the virtual mechanical time constant provided by the storage i during time t, and $T_{e,i,\max}$ is the maximum virtual mechanical time constant of storage i.

Energy storage can activate and deactivate the inertial support as needed, and Zhu et al. (2024) showed that the maximum inertial support power limit for the storage unit is given as

$$0 \le P^{H}_{e,i,\max} \le \frac{2T_{e,i,t}P^{dch}_{e,i,\max}f^{\max}_{RoCoF}}{f_0},$$

where $P^{H}_{e,i,\max}$ represents the maximum inertial support power of the energy storage i; $P^{dch}_{e,i,\max}$ represents the maximum discharge rate of the energy storage i; $f^{\max}_{RoCoF}$ denotes the maximum allowable decrease in the RoCoF at the initial moment.

To prevent secondary oscillations caused by the absorption of active power into the system when restoring the speed of the wind turbine after providing inertial support, Liu et al. (2016) proposed a control method to delay the restoration of the speed of the wind turbine until the system's PFR had responded fully. The active power required for wind turbine recovery is jointly borne by all PFR resources:

$$P^{H}_{w,i,\max} = \frac{2T_{w,i}P_{w,i,\max}f^{\max}_{RoCoF}}{f_0},$$

where $P^{H}_{w,i,\max}$ is the maximum inertial support power required for the wind turbine i, $T_{w,i}$ is the virtual mechanical time constant of the wind turbine i, and $P_{w,i,\max}$ is the maximum generation of the wind turbine i.

The total inertia of the system H_{system} is defined as

$$H_{system}(t) = \sum_{i=1}^{N_g} T_{g,i}P_{g,i,\max} + \sum_{i=1}^{N_w} T_{w,i}P_{w,i,\max} + \sum_{i=1}^{N_s} T_{e,i,t}P^{dch}_{e,i,\max},$$

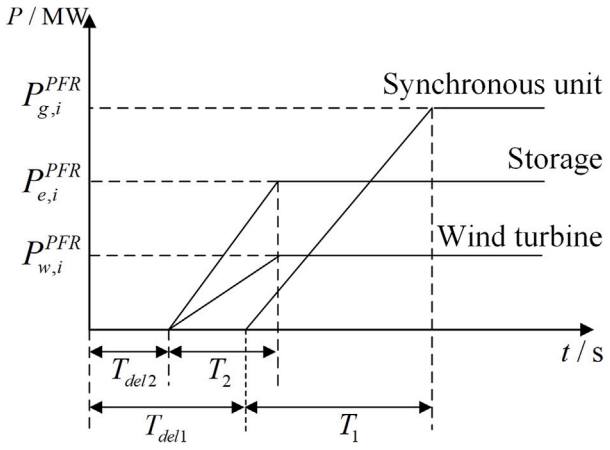

FIGURE 2
Dynamic frequency response of the primary frequency regulation (PFR) for each resource.

where $T_{g,i}$ represents the mechanical time constant of thermal unit i, and $P_{g,i,\max}$ is the maximum output of the thermal unit i.

Chu et al. (2020) proposed that the RoCoF is related to the active power shortage from the system disturbance and total inertia level of the system at the initial moment of power disturbance given by

$$f_{RoCoF} = \frac{df(t)}{dt}\Big|_{t=0^+} = \frac{f_0 P_{loss}}{2H_{system}} \le f^{\max}_{RoCoF},$$

where f_{RoCoF} represents the rate of frequency decrease at the initial moment.

2.4 Frequency nadir constraint with multiresource participation

Based on the assumptions that the synchronous unit, storage unit, and wind turbine PFR increase linearly at a certain ramp rate, their frequency response process is as shown in Figure 2. Zhu et al. (2024) showed that T_{del1} and T_{del2} are the response delays of the synchronous unit and storage unit PFR, while T_1 and T_2 are the ramp time constants of the synchronous unit and storage, respectively; these were based on the assumptions that the response delays and ramp time constants of the wind turbine and storage PFR are the same.

From Figure 2, the frequency nadir t^* is derived, which lies within $t \in [T_{del1}, T_{del1} + T_1]$:

$$t^* = \frac{(P_{loss} - P^{PFR}_s - P^{PFR}_w)}{\frac{P^{PFR}_g}{T_1}} + T_{del1}, \tag{2}$$

$$P^{PFR}_s = \sum_{i=1}^{N_s} P^{PFR,}_{e,i}$$

$$P^{PFR}_w = \sum_{i=1}^{N_w} P^{PFR,}_{w,i}$$

$$P^{PFR}_g = \sum_{i=1}^{N_g} P^{PFR}_{g,i},$$

where P_s^{PFR} is the total PFR capacity of the storage systems, P_w^{PFR} is the total PFR capacity of the wind turbines, and P_g^{PFR} is the total PFR capacity of the thermal units.

By integrating both sides of Equation 1, the expression for the frequency nadir is obtained as

$$\Delta f(t^*) = \frac{f_0}{2H_{system}} \cdot \left(\frac{P_g^{PFR}(t^* - T_{del1})^2}{2T_1} + \left(P_s^{PFR} + P_w^{PFR}\right)\left(t^* - T_{del2} - \frac{T_2}{2}\right) - P_{loss}t^* \right),$$

where $\Delta f(t^*)$ denotes the deviation at the frequency nadir.

The power shortage is fully compensated by the frequency modulation resources without considering load frequency modulation. Substituting Equation 2 above, the frequency nadir constraint can be obtained as

$$H_{system} \geq \frac{f_0}{2\Delta f_{\max}} \cdot \left(\frac{T_1 \cdot P_g^{PFR}}{2} - \left(P_s^{PFR} + P_w^{PFR}\right)\left(T_{del1} - T_{del2} - \frac{T_2}{2}\right) + P_{loss}T_{del1} \right),$$

where $\Delta f_{\max}$ denotes the maximum allowable frequency deviation.

2.5 Quasi-steady-state frequency constraint with multiresource participation

When the frequency drops to the nadir, power support is provided by the stored energy and synchronous PFR while ensuring that the total power from both sources exceeds the unbalanced power:

$$P_g^{PFR} + P_s^{PFR} \geq P_{loss} + \sum_{i=1}^{N_w} P_{w,i,\max}^H.$$

Thus, the following FSC sets are obtained:

$$\begin{cases} f_{RoCoF} = \dfrac{f_0 P_{loss}}{2H_{system}} \leq f_{RoCoF}^{\max} \\ H_{system} \geq \dfrac{f_0}{2\Delta f_{\max}} \cdot \left(\dfrac{T_1 P_g^{PFR}}{2} - \left(P_s^{PFR} + P_w^{PFR}\right)\left(T_{del1} - T_{del2} - \dfrac{T_2}{2}\right) + P_{loss}T_{del1} \right). \\ P_g^{PFR} + P_s^{PFR} \geq P_{loss} + \sum_{i=1}^{N_w} P_{w,i,\max}^H \end{cases}$$

3 Construction of VSCs in SCUC

3.1 Minimum short-circuit capacity requirement of buses

Based on the *Technical Regulations for Wind Farm Connection to Power System Part 1: Onshore Wind Power* (Gustavo and Gimenez, 2021), the requirement for low-voltage ride-through of wind power is proposed. When the short-circuit fault in the power grid is cut off for 1 s and voltage at the grid connection point reaches 0.9 p.u., the wind turbines are allowed to disconnect from the grid. To prevent disconnection of the wind turbines, it is necessary to maintain the minimum short-circuit capacity requirement of the renewable-energy grid-connected buses to suppress any transient voltage deviations; the smaller the short-circuit capacity, the more severe are the transient voltage deviations. The equivalent circuit of the renewable energy system is shown in Figure 3, where P_j and Q_j together represent the terminal power of the renewable energy system, U_i and U_j denote the initial and terminal voltages, respectively, and X_{eq} denotes the equivalent reactance of the system.

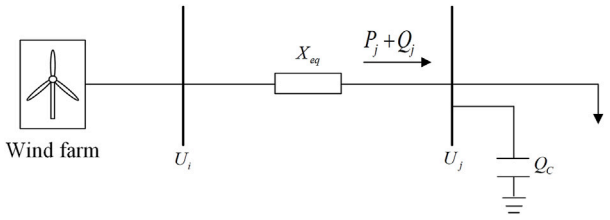

FIGURE 3
Equivalent circuit of the renewable energy system.

In the high-voltage grid, the resistance is neglected. Therefore, according to the voltage drop formula, the following can be derived:

$$\Delta U_j = \frac{Q_j X_{eq}}{U_j}, \tag{3}$$

where ΔU_j is the voltage deviation of bus j.

Next, we set the short-circuit capacity $S_{ac,j}$ of the bus j as follows:

$$S_{ac,j} = \frac{U_i^2}{X_{eq}}. \tag{4}$$

Using approximate algorithms and substituting Equation 3 into Equation 4, we obtain the simplified expression for the short-circuit capacity of bus j as

$$\Delta U_j = \frac{\Delta Q_j U_i^2}{S_{ac,j} U_j},$$

where ΔQ_j is the reactive power deviation of bus j before and after the fault.

With the assumption that $U_i \approx U_j$, the expression for ΔU_j is simplified as follows:

$$\Delta U_j = \frac{\Delta Q_j U_j}{S_{ac,j}}.$$

During the short-circuit fault, the active power provided by the unit is zero, so the reactive power margin Q_j of the system during the fault is the reactive compensation amount during normal operation of the system. That is, $Q_C = \Delta Q_j$, and the reactive power compensation of the renewable-energy grid-connected buses during normal operation is approximately 20%–40% of the active power transmitted by the line (Xu et al., 2015). The reactive power surplus of the buses meets the following requirement with its transmitted active power:

$$Q_C = \rho P_j,$$

where P_j is the output power of the renewable energy bus j.

The maximum voltage deviation allowed for the buses connected to renewable energy sources during faults is 0.1 p.u. Therefore, the minimum short-circuit capacity requirement of the bus can be derived as follows:

$$S_{ac,j,\min} = 10\rho P_j, \tag{5}$$

where $S_{ac,j,\min}$ is the minimum short-circuit capacity requirement for bus j.

3.2 VSCs based on short-circuit capacity

The short-circuit capacity of each bus in the system depends on the network structure and start–stop status of each unit. The equivalent impedances of different units to different buses vary along with the short-circuit capacities that they provide. To adapt to the algorithm and obtain linear constraints, it is necessary to quantify the short-circuit capacities provided by different units to different buses. Using the short-circuit capacity conversion coefficient, the short-circuit current provided by each synchronous unit to each bus is weighted, thereby associating the start–stop status of that unit with the short-circuit capacity of the corresponding bus.

The short-circuit capacity of a bus is the product of its rated voltage U_N and the three-phase short-circuit fault current I_f, as shown below:

$$S_{ac} = U_N I_f. \tag{6}$$

As the unit values of the short-circuit capacity and short-circuit current are equal, only the short-circuit current I_f of Equation 6 is required to obtain the short-circuit capacity provided by the unit to the bus. Consequently, the higher the short-circuit current of the bus, the larger is its short-circuit capacity and stronger is the voltage support capacity. The short-circuit capacity of the system is primarily provided by the synchronous units, and the impacts of renewable energy units on the bus short-circuit capacity are relatively minor. Therefore, we primarily consider only the impacts of the synchronous units and storages on the bus short-circuit capacity. The short-circuit capacity provided by each unit to a specific bus is related to the electrical distance between them, so a linear integer short-circuit capacity constraint is obtained to maintain the system voltage within a reasonable range after a fault. To reasonably configure the starts and stops of the units, it is necessary to calculate the short-circuit capacity conversion coefficient of each unit to each bus and obtain the linear constraints, so that the SCUC algorithm can be used to optimize the startup modes of the synchronous units while meeting certain economic requirements and ensuring transient voltage stability of the system.

Owing to the large short-circuit currents provided by the synchronous units to the system, the electrical distance between each unit and each bus can be represented by the network reactance matrix. This matrix can be used to calculate the short-circuit current provided by each unit to each bus. To calculate the short-circuit capacity provided by the synchronous unit i to bus j, the internal electromotive forces of all other units in the system are set to zero, so that the rated voltage of the synchronous unit i is the system rated voltage. Then, the short-circuit current $I_{i,j}$ provided by the synchronous unit i to bus j under the rated operating conditions is calculated as follows:

$$\begin{bmatrix} I_{i,1} \\ \vdots \\ I_{i,j} \\ \vdots \\ I_{i,N} \end{bmatrix} = \mathbf{B} \begin{bmatrix} 0 \\ 0 \\ U_{i,e} \\ 0 \\ 0 \end{bmatrix} = \mathbf{X}^{-1} \begin{bmatrix} 0 \\ 0 \\ U_{i,N} \\ 0 \\ 0 \end{bmatrix},$$

where $U_{i,N}$ denotes the rated voltage of thermal unit i, matrix $\mathbf{B}$ is the network admittance matrix of the system, and matrix $\mathbf{X}$ is the network reactance matrix of the system.

The short-circuit capacity $S_{i,j}$ provided by unit i to bus j at the rated voltage is

$$S_{i,j} = I_{i,j} U_{i,N}.$$

To ensure that each system bus has sufficient short-circuit capacity to maintain the transient voltage stability in the event of a fault, it is necessary to ensure that the short-circuit capacity $S_{i,j}$ provided by each unit to a certain bus is not below a minimum value (i.e., the minimum short-circuit capacity requirement of the bus), and the calculated short-circuit capacity will differ from the actual value. Therefore, a correction factor M_s must be considered. Based on virtual synchronous generator (VSG) technology, the impact characteristics of grid-type storage on voltage are similar to those of synchronous units. The sum of the short-circuit capacities provided by the synchronous units and energy storage systems on the buses is given by

$$M_s \left(\sum_{i=1}^{N_g} S_{i,j} u_{g,i,t} + \sum_{i=1}^{N_s} S_{e,i,j} \right) \geq S_{\mathrm{ac,j,\,min}},\ j = 1, 2, \ldots, N_{\mathrm{k}},$$

where N_k denotes the total number of renewable-energy grid-connected buses, and M_s is estimated from the actual operating conditions as 0.89 (Niu et al., 2021).

The short-circuit capacity provided by storage i to bus j at the rated voltage is

$$S_{e,i,j} = I_{e,i,j} U_{e,i,N},$$

where $I_{e,i,j}$ is the short-circuit current provided by storage i to bus j at the rated voltage, and $U_{e,i,N}$ is the rated voltage of the bus j where storage i is located.

4 FVS-SCUC model with energy storage and wind turbine participation

4.1 Objective function

Considering the coal consumption costs of thermal units, startup and shutdown costs of thermal units, operation and maintenance costs of wind turbines, compensation costs for energy storage charging and discharging, compensation costs for PFR of energy storage, and compensation costs for energy storage inertial services, the objective function can be obtained as shown in Equation (7):

$$f = \sum_{i=1}^{N_g}\sum_{t=1}^{T}\left[\left(a_i P_{g,i,t}^2 + b_i P_{g,i,t} + c_i\right) + \left(u_{g,i,t}\left(1 - u_{g,i,(t-1)}\right)C_{i,start}\right) + \left(u_{g,i,(t-1)}\left(1 - u_{g,i,t}\right)C_{i,shutdown}\right)\right] + \left(\sum_{i=1}^{N_w} C_{w,i}\sum_{t=1}^{T} P_{w,i,t} + \sum_{i=1}^{N_s} C_{e,i}^{ch}\sum_{t=1}^{T} P_{e,i,t}^{ch} + \sum_{i=1}^{N_s} C_{e,i}^{dch}\sum_{t=1}^{T} P_{e,i,t}^{dch} + \sum_{i=1}^{N_s} C_{PFR,e}\sum_{t=1}^{T} P_{e,i,t}^{PFR} + \sum_{i=1}^{N_s} C_e^H \sum_{t=1}^{T} P_{e,i,t,\max}^{H}\right)\Delta t \quad (7)$$

Here, T is the total number of time periods in the scheduling cycle, which is 24; a_i, b_i, and c_i are the coal consumption cost coefficients of the thermal unit i; $P_{g,i,t}$ is the output of the thermal unit i during time period t; $P_{w,i,t}$ is the output of the wind turbine i during time period t; $u_{g,i,t}$ is the online and offline status of the thermal unit i during time period t, where $u_{g,i,t} = 1$ implies online and $u_{g,i,t} = 0$ indicates offline; $C_{i,start}$ and $C_{i,shutdown}$ are the single startup and shutdown cost coefficients of the thermal unit i; $C_{w,i}$ is the operation cost coefficient of the wind turbine i; $P_{w,i,t}$ is the active output of the wind turbine i during time period t; $C_{e,i}$ is the charging and discharging cost coefficient of energy storage i; $P_{e,i,t}^{ch}$ is the charging rate of energy storage i during time period t; $P_{e,i,t}^{dch}$ is the discharging rate of energy storage i during time period t; $C_{PFR,e,i}$ is the unit frequency modulation compensation cost coefficient for energy storage i; $P_{e,i,t}^{PFR}$ is the PFR output of energy storage i during time period t.

4.2 System-level constraints

4.2.1 Power balance constraint

The system must meet the power balance at each time period t as follows:

$$\sum_{i=1}^{N_g} P_{g,i,t} + \sum_{i=1}^{N_w} P_{w,i,t} + \sum_{i=1}^{N_s}\left(P_{e,i,t}^{dch} - P_{e,i,t}^{ch}\right) = \sum_{i=1}^{N_L} P_{L,i,t}$$

where N_L is the number of load buses, and $P_{L,i,t}$ is the active power demand of load i during time period t.

4.2.2 Active reserve constraint

When addressing the power deficit and outage of the largest-capacity unit, the active power reserved by the system is given as

$$\sum_{i=1}^{N_g} u_{g,i,t}\left(P_{g,i,\max} - P_{g,i,t}\right) \geq \max\left\{\lambda\sum_{i=1}^{N_L} P_{L,i,t}, P_{g,i,\max}, \ldots\right\},$$

where λ is the reserve coefficient. The reserve capacity allocated to the power system should be larger than the capacity of the largest unit in the system.

4.2.3 Network security constraint

The power flowing through line l should be less than its maximum transmission power. The element $A_{j,l}$ of the bus reactance matrix is used to reflect the simple linear relationship between the injected power of bus j and active power of branch l as follows:

$$-P_{l,\max} \leq \sum_{j=1}^{N} A_{j,l}\left(P_{g,j,t} + P_{w,j,t} - P_{L,j,t} + P_{e,j,t}^{dch} - P_{e,j,t}^{ch}\right) \leq P_{l,\max}$$
$$t = 1, \ldots, T \quad l = 1, \ldots, N_{b,}$$

where N is the number of buses; $A_{j,l}$ is the sensitivity coefficient of bus j to line l; $P_{g,j,t}$ is the output of the thermal unit during time period t at bus j; $P_{w,j,t}$ is the output of the wind turbine during time period t at bus j; $P_{L,j,t}$ is the active demand of the load during time period t at bus j; $P_{e,j,t}^{ch}$ is the charging rate of energy storage during time period t at bus j; $P_{e,j,t}^{dch}$ is the discharging rate of energy storage during time period t at bus j; $P_{l,\max}$ is the maximum power transmission capacity of line l; N_b is the number of branches.

4.2.4 FSC set

Based on the derivations in Section 2, the obtained FSC set is as follows:

$$\begin{cases} f_{RoCoF} = \dfrac{f_0 P_{loss}}{2H_{system}} \leq f_{RoCoF}^{\max} \\ H_{system} \geq \dfrac{f_0}{2\Delta f_{\max}} \cdot \left(\dfrac{T_1 P_g^{PFR}}{2} - \left(P_s^{PFR} + P_w^{PFR}\right)\left(T_{del1} - T_{del2} - \dfrac{T_2}{2}\right) + P_{loss} T_{del1}\right). \\ P_g^{PFR} + P_s^{PFR} \geq P_{loss} + \sum_{i=1}^{N_w} P_{w,i,\max}^{H} \end{cases}$$

4.2.5 VSCs

Based on VSG technology, energy storage devices provide a certain short-circuit capacity support to the fault point at the moment of failure; considering the storage, the maximum output power P_j of the renewable energy channel will change, such that the minimum short-circuit capacity demand is affected. To ensure adequate short-circuit capacity of the bus, the sum of the short-circuit capacities provided by the grid-connected units should not be less than the required minimum as follows:

$$M_s\left(\sum_{i=1}^{N_g} S_{i,j} u_{g,i,t} + \sum_{i=1}^{N_s} S_{e,i,j}\right) \geq S_{\text{ac,j,min}}, \quad j = 1, 2, \ldots, N_{\text{k}}.$$

If the short-circuit capacity provided by grid-type energy storage is not considered, the above expression becomes

$$M_s\sum_{i=1}^{N_g} S_{i,j} u_{g,i,t} \geq S_{\text{ac,j,min}}, \quad j = 1, 2, \ldots, N_{\text{k.}}$$

4.3 Constraints related to thermal power units

4.3.1 Power output constraints of thermal power units

The thermal power unit i must have a reserve for PFR, which is given by

$$u_{g,i,t} P_{g,i,\min} \leq P_{g,i,t} \leq u_{g,i,t} P_{g,i,\max} - u_{g,i,t} P_{g,i,t,}^{PFR}$$

where $P_{g,i,\min}$ is the minimum active output of the thermal unit i, and $P_{g,i,t}^{PFR}$ is the PFR output of thermal unit i during time period t.

4.3.2 Climbing constraints for thermal power units

This work distinguishes between the climbing rate during the operating period of the thermal power unit and that during the startup and shutdown periods, whose constraints are as follows:

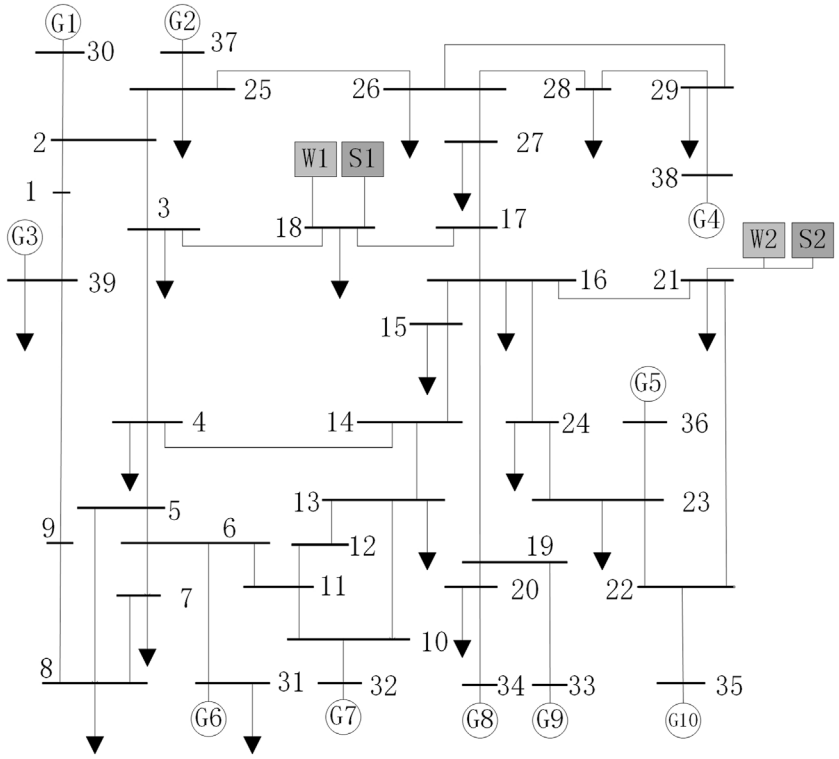

FIGURE 4
Improved IEEE-39 system architecture diagram.

$$\begin{cases} P_{g,i,t} - P_{g,i,(t-1)} \le u_{g,i,t-1} R_{i,up} + \left(1 - u_{g,i,t-1}\right) R_{i,startup} \\ P_{g,i,(t-1)} - P_{g,i,t} \le u_{g,i,t} R_{i,down} + \left(1 - u_{g,i,t}\right) R_{i,shutdown}, \end{cases}$$

where $R_{i,up}$ and $R_{i,down}$ are the maximum upward and downward ramping capacities of the thermal unit i, respectively. $R_{i,startup}$ and $R_{i,shutdown}$ are the maximum startup and shutdown ramping capacities of the thermal unit i, respectively, which are given by $(P_{g,i,\max} + P_{g,i,\min})/2$.

4.3.3 Time constraints for starting and stopping thermal power units

The running and shutdown times of a thermal power unit i should be larger than their minimum allowable on/off times as follows:

$$\begin{cases} \sum_{k=t}^{t+X_{S,i}-1} \left(1 - u_{g,i,k}\right) \ge T_{S,i} \left(u_{g,i,(t-1)} - u_{g,i,t}\right) \\ \sum_{k=t}^{t+X_{O,i}-1} u_{g,i,k} \ge T_{O,i} \left(u_{g,i,t} - u_{g,i,(t-1)}\right) \end{cases},$$

where $X_{S,i}$ and $X_{O,i}$ are the scheduled minimum offline and online hours of the thermal unit i, and $T_{S,i}$ and $T_{O,i}$ are the actual offline and online hours of the thermal unit i, respectively.

4.4 Wind turbine output constraints

Based on VSG technology, the rotational inertia of a wind turbine transmission shaft system can provide certain inertial support to the system. In addition, Kuang et al. (2022) proposed that wind power needs a reserve capacity in the output to provide PFR to the power system.

The output constraints of a wind turbine are related to the capacity constraints of PFR as follows:

$$0 \le P_{w,i,t} \le P_{w,i,t,pre} - P^{PFR}_{w,i,t,}$$
$$0 \le P^{PFR}_{w,i,t} \le \varepsilon_{w,i} P_{w,i,t,pre},$$

where $P^{PFR}_{w,i,t}$ is the PFR output of the wind turbine i during time period t; $P_{w,i,t,pre}$ is the predictive active output of the wind turbine i during time period t; $\varepsilon_{w,i}$ is the proportional coefficient of the PFR capacity of the wind turbine i, whose value is 0.1.

4.5 Energy-storage-related constraints

4.5.1 Energy storage charging constraint

The charging power of energy storage is limited by its maximum and minimum values, and a certain margin of this value needs to be left as a reserve for PFR and inertial support of energy storage (Zhu et al., 2024):

$$P^{ch}_{e,i,\min} \cdot \alpha_{c,e,i,t} + P^{PFR}_{e,i,t} + P^{H}_{e,i,\max} \le P^{ch}_{e,i,t} \le P^{ch}_{e,i,\max} \cdot \alpha_{c,e,i,t},$$

where $P^{ch}_{e,i,\min}$ is the minimum charging rate of energy storage i; $P^{ch}_{e,i,\max}$ is the maximum charging rate of energy storage i; $\alpha_{c,e,i,t}$ is the

TABLE 2 Thermal power unit parameters.

Thermal unit	Bus	P_{max} (MW)	P_{min} (MW)	a ($·MW^{-2}$)	b ($·MW^{-1}$)	c ($)	$R_{i,up}/R_{i,down}$ $R_{i,startup}$ $/R_{i,shutdown}$ ($MW·h^{-1}$)	$T_{S,i}/T_{O,i}$ (h)	$C_{i,start}/C_{i,shutdown}$ ($/time)	$T_{g,i}$ (s)
1	30	1,000	500	0.2	55	1,035	700	2	220,000	10
2	37	1,000	500	0.2	55	1,035	700	2	250,000	10
3	39	1,000	450	0.15	50	965	670	2	270,000	9.5
4	38	800	400	0.3	70	1,240	550	2	200,000	8.5
5	36	1,000	500	0.2	55	1,075	700	2	230,000	8.5
6	31	850	420	0.15	50	965	600	2	210,000	7.5
7	32	1,000	500	0.4	75	1,310	700	2	220,000	8
8	34	600	300	0.12	40	825	400	2	140,000	6
9	33	600	300	0.45	85	1,380	400	2	150,000	6.5
10	35	600	300	0.25	60	1,175	400	2	160,000	6

TABLE 3 Wind turbine parameters.

Wind turbine	Bus	$P_{w,i,max}$ (MW)	$C_{W,i}$ ($/MWh)	$T_{w,i}$(s) (Zhu et al., 2024b)
1	18	1,800	45	2
2	21	1,800	40	2

TABLE 4 Energy storage parameters.

Storage	Bus	S_{max} (MWh)	S_{min}(MWh)	S_0 (MWh)	$P_{ch,max}$ (MW)
1	18	1,000	400	600	400
2	21	1,000	400	600	500
	$P_{ch,min}$ (MW)	$P_{dch,max}$ (MW)	$P_{dch,min}$ (MW)	$C_{e,i,dch}$ ($/MWh)	$C_{e,i,ch}$ ($/MWh)
1	0	400	0	140	110
2	0	500	0	140	110
	$C_{PFR,e,i}$ ($/MWh)	$C_{H,e,i}$ ($/MWh)	η	$T_{e,i,max}$(s) (Zhu et al., 2024b)	$T_{e,i,min}$(s)
1	165	165	0.95	2	0
2	165	165	0.95	2	0

charging state variable of energy storage i during time period t, whose value is either 0 or 1.

4.5.2 Energy storage discharging constraint

The discharging power of energy storage is constrained by not only the maximum and minimum discharge power limits but also a certain margin that must be left as reserve for PFR and inertial support of energy storage (Zhu et al., 2024):

$$P^{dch}_{e,i,\min} \cdot \alpha_{d,e,i,t} \le P^{dch}_{e,i,t} \le P^{dch}_{e,i,\max} \cdot \alpha_{d,e,i,t} - P^{PFR}_{e,i,t} - P^{H}_{e,i,\max},$$

$$0 \le P^{PFR}_{e,i,t} \le \varepsilon_{e,i} P^{dch}_{e,i,\max},$$

$$0 \le P^{dch}_{e,i,\max},$$

where $P^{dch}_{e,i,\min}$ is the minimum discharging rate of energy storage i; $\alpha_{d,e,i,t}$ is the discharging state variable of energy storage i during time period t; $\varepsilon_{e,i}$ is the proportional coefficient of the PFR capacity of energy storage i, whose value is 0.1.

4.5.3 State of charge (SoC) capacity constraint

A portion of the energy storage capacity is often maintained as reserve for PFR and inertial support, and the reserve capacity supported by the energy storage short-circuit capacity is

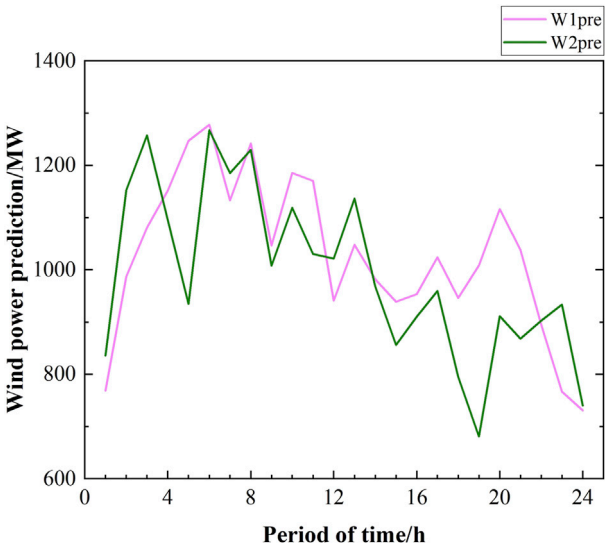

FIGURE 5
Wind power prediction.

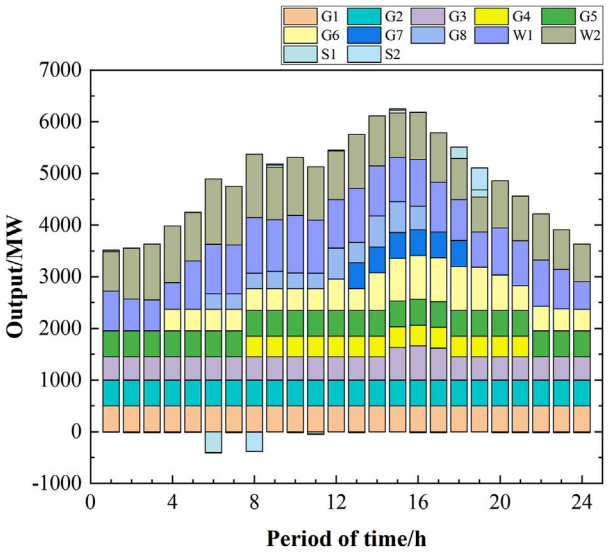

FIGURE 7
Unit commitment plan for each unit during each time period in scenario 2.

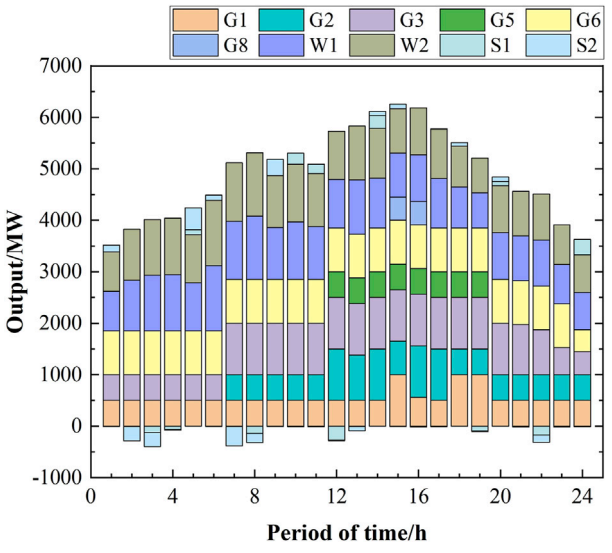

FIGURE 6
Unit commitment plan for each unit during each time period in scenario 1.

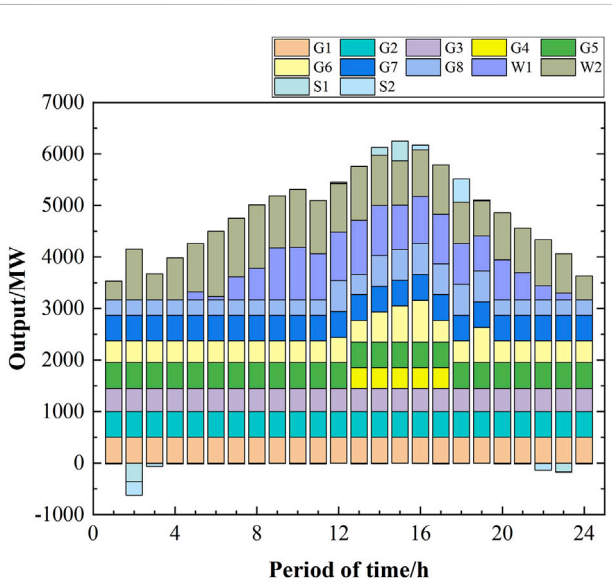

FIGURE 8
Unit commitment plan for each unit during each time period in scenario 3.

neglected owing to the instantaneous character of short-circuit capacity support:

$$S_{e,i,\min}^{SoC} + S_{e,i,t}^{res} \le S_{e,i,t}^{SoC} \le S_{e,i,\max}^{SoC},$$

$$S_{e,i,t}^{res} = \frac{S_{e,i,t}^{H} + S_{e,i,t}^{PFR} + S_{e,i,t}^{V}}{S_{e,i,N}},$$

$$0 \le S_{e,i,t}^{H} \le \frac{2T_{e,i,t} f_{RoCoF}^{\max} \Delta t}{f_0},$$

$$S_{e,i,t}^{PFR} = \frac{T_2 P_{e,i,t}^{PFR}}{2},$$

$$S_{e,i,t}^{V} = \Delta T \cdot S_{e,i,j},$$

where $S_{e,i,t}^{SoC}$ is the remaining electrical energy in energy storage i during time period t; $S_{e,i,N}$ is the rated capacity of energy storage i; $S_{e,i,t}^{H}$ is the amount of electricity required for inertial support provided by energy storage i during time t; $S_{e,i,t}^{PFR}$ is the amount of electricity required for PFR provided by energy storage i during time t; $S_{e,i,t}^{V}$ is the amount of electricity required for voltage support services provided by energy storage i during time t; $S_{e,i,\min}^{SoC}$ is the minimum allowable energy margin of energy storage i; $S_{e,i,\max}^{SoC}$ is the

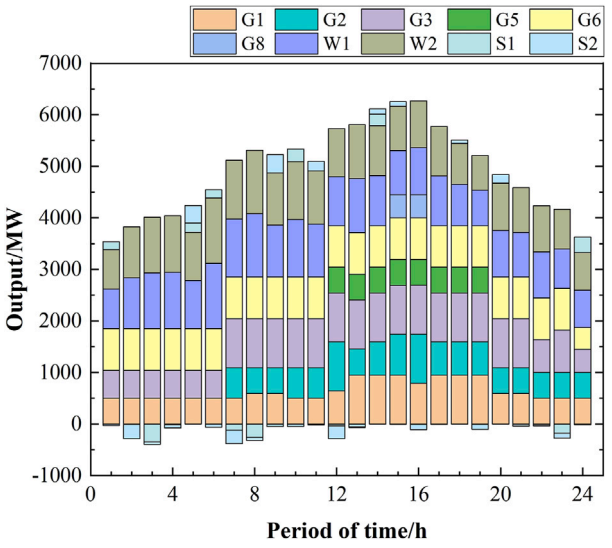

FIGURE 9
Unit commitment plan for each unit during each time period in scenario 4.

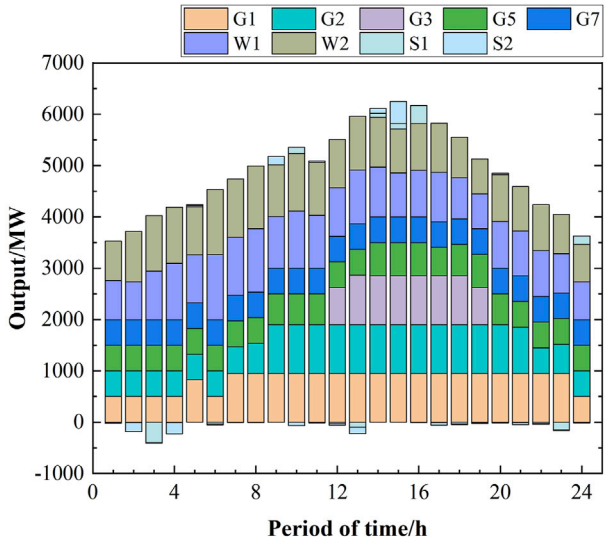

FIGURE 10
Unit commitment plan for each unit during each time period in scenario 5.

maximum allowable energy margin of energy storage i; $S_{e,i,t}^{res}$ is the reserve capacity of energy storage i for time period t; ΔT is the fault duration.

4.5.4 SoC operational constraint

The remaining capacity state of energy storage is limited; thus, the initial value of the electrical energy for the next period during operation is equal to the electrical energy at the end of the previous period, and the electrical energy at the initial time period is equal to that at the final time period. Since the constraints on energy storage charging and discharging consider the active power output required for inertial services and PFR, these factors are not considered again below to avoid duplication:

$$S_{e,i,t}^{SoC} = S_{e,i,t-1}^{SoC} + \frac{\eta_i P_{e,i,t}^{ch} \Delta t}{S_{e,i,N}} - \frac{P_{e,i,t}^{dch} \Delta t}{\eta_i S_{e,i,N}},$$
$$S_{e,i,0}^{SoC} = S_{e,i,T,}^{SoC}$$

where $S_{e,i,t-1}^{SoC}$ is the energy margin of energy storage i during time period $t-1$; η_i is the charging and discharging efficiency of energy storage i, whose value is 0.95; $S_{e,i,0}^{SoC}$ is the initial capacity of energy storage i; $S_{e,i,T}^{SoC}$ is the remaining energy of energy storage i at the end period.

5 Example analysis

In this study, the enhanced IEEE-39 system was selected for numerical analyses. The corresponding model was established using MATLAB 2021a, and the CPLEX software is called using YALMIP. Linear programming and iterative methods were used to solve the model, and the steps for the solution are as follows:

1. Determine the UCs of the prestart units based on the conventional constraints (i.e., system and individual unit constraints).
2. In the prestartup UCs determined in step 1, calculate the inertial and short-circuit capacities provided by each unit to meet the frequency and voltage stability constraints as well as solve the startup scheme that meets the stability constraints.
3. If the final UC scheme in step 2 meets the power flow security constraints, then output the result; if not, return to step 1 for recalculation.

Two wind turbines and two energy storage units were installed at buses 18 and 21, respectively. The system structure is shown in Figure 4, and the parameter settings and system parameters of each unit are shown in Tables 2–4; the parameters of the thermal power unit used in this work are based on Yang et al. (2020), and the practical values of the parameters were ensured. The wind power prediction is shown in Figure 5; here, ρ value was considered 0.4 when the short-circuit capacity provided by the energy storage was not included. The minimum short-circuit capacity requirements for buses 18 and 21 as calculated using Equation 5 are 5,449.8 MW and 6,431.3 MW, respectively. After considering the short-circuit capacities provided by energy storage, the minimum short-circuit capacity requirements for buses 18 and 21 as calculated using Equation 5 are 5,858.7 MW and 5,318.6 MW, respectively.

The disturbance in each time period is set to a sudden increase of 5% of the total load in the corresponding time period, and the reserve coefficient of each thermal unit is set to 5%. The rated frequency of the system is 50 Hz, maximum RoCoF value is 1 Hz/s, and maximum frequency deviation is 1 Hz (National Energy Administration, 2021). The delay of storage PFR T_{del2} is 0.5 s, and the total response time T_2 is 2 s; the synchronization unit PFR

TABLE 5 Mutual reactance between the renewable energy and thermal unit bus (Ω).

Renewable bus \ Thermal bus	30 (1)	31 (6)	32 (7)	33 (9)	34 (8)	35 (10)	36 (5)	37 (2)	38 (4)	39 (3)
18	9.28	9.04	8.99	8.62	8.62	9.06	9.29	9.34	9.75	10.26
21	9.65	9.10	8.99	8.01	8.01	7.56	7.92	9.67	9.97	10.50

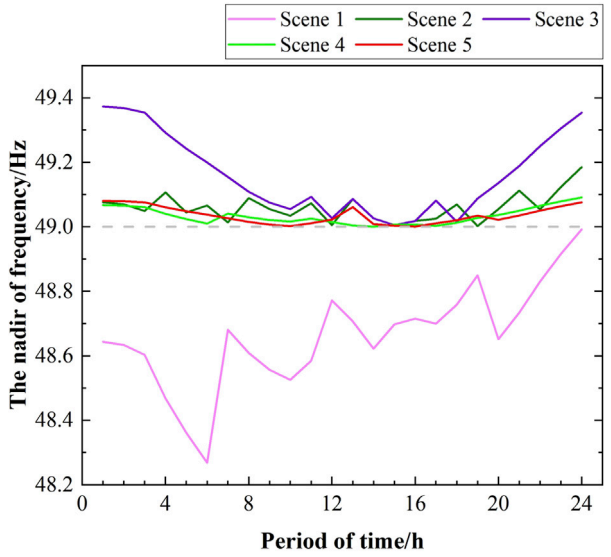

FIGURE 11
Frequency nadir of the system during each time period in the five scenarios.

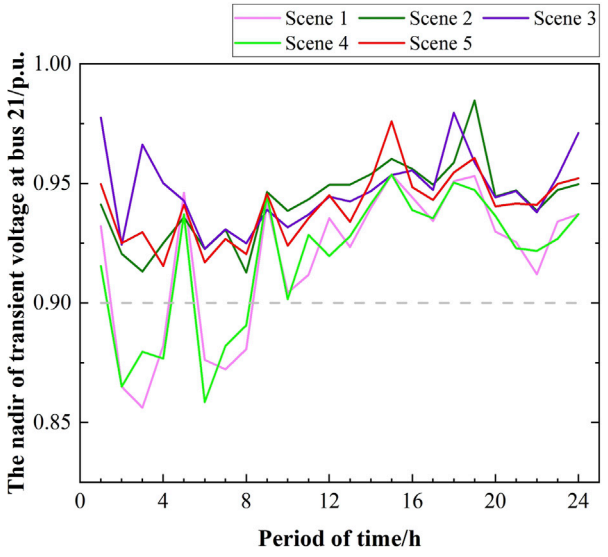

FIGURE 13
Nadir of the transient voltage at bus 21 during each time period in the five scenarios.

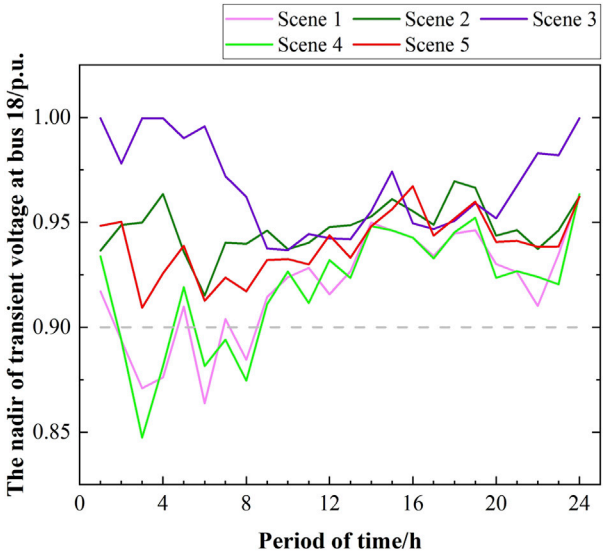

FIGURE 12
Nadir of the transient voltage at bus 18 during each time period in the five scenarios.

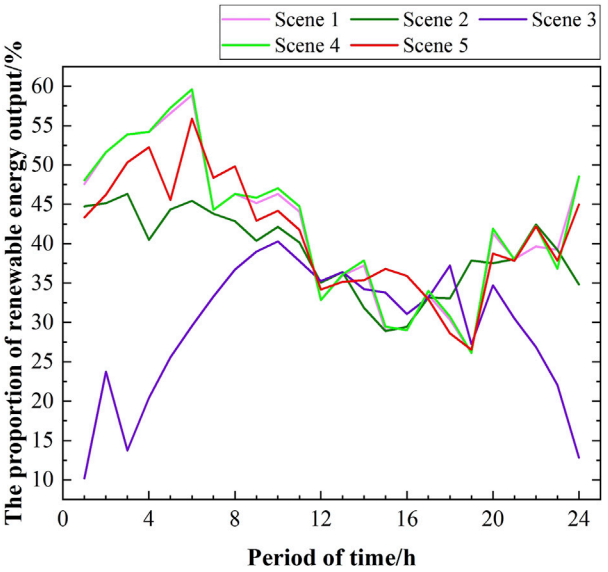

FIGURE 14
Proportion of renewable energy during each time period in the five scenarios.

TABLE 6 System costs in the five scenarios.

	Total system cost (×10^5$)	Startup and shutdown costs (×10^5$)	Storage cost (×10^5$)	Wind turbine cost (×10^5$)
Scenario 1	620.85	16.90	6.42	19.53
Scenario 2	871.57	23.00	2.97	18.51
Scenario 3	983.74	19.40	3.24	14.46
Scenario 4	621.95	16.90	9.78	19.53
Scenario 5	690.61	14.60	6.74	19.36

delay T_{del1} is 3 s, and the total response time T_1 is 10 s (Zhu et al., 2024).

Comparative analyses were then conducted for the following five scenarios:

Scenario 1: SCUC involving storages and wind turbines;
Scenario 2: FCUC without storages and wind turbines involved in frequency regulation;
Scenario 3: FVS-SCUC without storages and wind turbines involved in frequency and voltage regulations;
Scenario 4: FCUC involving storages and wind turbines;
Scenario 5: FVS-SCUC involving storages and wind turbines.

The UC planning of each unit during each time period of the system, as solved in scenarios 1 to 5 are shown in Figures 6–10, respectively. Based on the principle of prioritizing the startups of units with lower coal consumption and startup costs, units 1, 2, and 3 had the highest numbers of open times. A comparison between scenarios 1 and 3 reveals that the system must increase the number of thermal units that need to be opened to meet the minimum inertial and short-circuit capacity requirements. Thus, the system activated units 4 and 7 during the peak load periods. A comparison of scenarios 2 and 3 reveals that the minimum short-circuit capacity requirement constraint necessitated opening of units 6, 7, and 8 during periods of low loads. This resulted in significant curtailment of wind power generation during these periods. Furthermore, the high costs of charging energy storage meant that they were unable to fully absorb the wind power output.

A comparison of the UC planning of scenarios 2 and 4 reveals the impact characteristics of energy storage and wind turbines on the frequency, which reduced the frequency regulation burden of the thermal power units. Consequently, the number of thermal unit opening times in scenario 4 decreased. Similarly, comparing the UC planning of scenarios 3 and 5 by considering the impact of energy storage on the short-circuit capacity, it is seen that the voltage regulation burden of the thermal power units is reduced, resulting in a decrease in the number of startup units in scenario 5 compared to scenario 3. Conversely, the curtailed wind power in scenarios 4 and 5 decreased. A comparison of scenarios 4 and 5 reveals that when VSCs are considered, the operations shift from units 3 and 6 to units 2, 5, and 7 during periods of low loads. As shown in Table 5, the reason for this shift is that units 5 and 7 exhibit lower reactances to the renewable-energy grid-connected buses, thereby reducing the electrical distance. Moreover, these units have greater maximum capacities, enabling them to provide robust voltage support to the buses.

As shown in Figures 11–13, scenarios 3 and 5 demonstrate that the frequency and voltage are within the prescribed limits. Similarly, scenarios 2 and 4 satisfy the frequency constraints. In contrast, scenario 1 fails to meet both the frequency and voltage constraints. The results of scenario 2 in Figure 12 demonstrate that the generation plan is capable of meeting the minimum short-circuit demands of the buses and maintaining the transient voltage above 0.9 p.u.; this indicates that FSC is an effective constraint in this scenario. It can be observed that the transient voltage stability criterion is not met in scenario 4.

The proportion of renewable energy output in each scene is shown in Figure 14. Because of consideration of the frequency and voltage stability constraints, the number of thermal units increased, resulting in decreases in the outputs of the wind turbines. In most of the time periods, scenario 3 exhibited the lowest proportion of renewable energy output. Scenario 5 considers the frequency and voltage regulation effects of the storage and wind turbines; compared to scenario 3, the number of thermal units opened had reduced, and the proportion of renewable energy output had increased.

As shown in Table 6, in scenarios 2 and 3, owing to consideration of the frequency and voltage stability constraints, the startups of high-cost thermal units significantly increased the total cost of the system compared to scenario 1. In scenarios 4 and 5, after considering the constraints from energy storage and wind turbine participation in the frequency and voltage stabilities, the burden on the thermal units for frequency and voltage regulations reduced. Consequently, the numbers of startup and shutdown operations of these units decreased, leading to reduced startup costs compared to scenarios 2 and 3. Moreover, the total system cost decreased.

However, with the incorporation of energy storage for frequency regulation and inertial services, the PFR costs and daily charging/discharging power increase, resulting in elevated energy-storage-related costs in scenarios 4 and 5 than scenarios 2 and 3. Although wind turbine curtailment occurs in scenarios 2 and 3, resulting in reduced wind turbine costs, there is no curtailment in scenario 4. This wind curtailment, in conjunction with the consideration of energy storage and wind turbine participation in the frequency and voltage stabilities, enhances the economic efficiency of the system.

In scenarios 4 and 5, the numbers of thermal units opened increased due to the consideration of VSCs in scenario 5, resulting in wind curtailment and subsequent decrease in the storage and wind turbine costs compared to scenario 4. The reduced number of unit shutdowns in scenario 5 resulted in reduced startup and shutdown costs compared to those in scenario 4.

6 Conclusion

This study addresses the challenges of frequency and voltage instabilities in renewable energy systems due to reductions in the number of thermal power units being started after large-scale integration of renewable energy sources. Consequently, we propose an SCUC model considering frequency and voltage stabilities by taking into account the impacts of energy storage and wind turbine generators on the frequency and voltage stabilities. The following conclusions can be drawn:

(1) Based on the assumption that the PFR output of each resource in the system increases linearly over time, incorporating the derived FSCs into the SCUC can ensure frequency stability.
(2) It is necessary to include VSCs in the SCUC. Once the short-circuit faults are cleared, it is necessary to enhance the voltage support capabilities and suppress transient voltage deviations at the wind turbine buses to prevent disconnection of the wind turbines from the grid.
(3) Further consideration of the impacts of energy storage and wind turbine generators on the frequency and voltage stability constraints in the FVS-SCUC allows reduction in the total cost of the system and a decrease in wind curtailment, thereby improving the economic efficiency of the system.
(4) Compared to methods proposed by other scholars, the approach presented herein considers the short-circuit capacities provided by all units in the grid buses by incorporating energy storage considerations. This approach allows linearized VSCs; further, the proposed method is computationally straightforward and suitable for formulating day-ahead generation schedules in large-scale power grids.

Data availability statement

The original contributions presented in this study are included in the article/Supplementary Material, and any further inquiries may be directed to the corresponding author.

Author contributions

ZZ: Writing–original draft, Writing–original editing. ZJ: Conceptualization, Formal analysis, Methodology, Resources, Writing–original draft, Writing–original editing.

Funding

The author declares that no financial support was received for the research, authorship, and/or publication of this article.

Conflict of interest

The author declares that the research was conducted in the absence of any commercial or financial relationships that could be construed as a potential conflict of interest.

Publisher's note

References

Badesa, L., Teng, F., and Strbac, G. (2019). Simultaneous scheduling of multiple frequency services in stochastic unit commitment. *IEEE Trans. Power Syst.* 34 (5), 3858–3868. doi:10.1109/tpwrs.2019.2905037

Badesa, L., Teng, F., and Strbac, G. (2021a). Conditions for regional frequency stability in power system scheduling—part i: theory. *IEEE Trans. Power Syst.* 36 (6), 5558–5566. doi:10.1109/tpwrs.2021.3073083

Badesa, L., Teng, F., and Strbac, G. (2021b). Conditions for regional frequency stability in power system scheduling—part ii: application to unit commitment. *IEEE Trans. Power Syst.* 36 (6), 5567–5577. doi:10.1109/tpwrs.2021.3073077

Chu, Z., Markovic, U., Hug, G., and Teng, F. (2020). Towards optimal system scheduling with synthetic inertia provision from wind turbines. *IEEE Trans. Power Syst.* 35 (5), 4056–4066. doi:10.1109/tpwrs.2020.2985843

Fu, X., Cui, J., Wang, C., Song, X., and Sun, Y. (2024). Transient overvoltage risk assessment considering the short-circuit ratio of multiple renewable energy stations [J/OL]. *J. Power Syst. Automation*, 1–10. Available at: http://doi.org.shiep.vpn358.com/10.19635/j.cnki.csu-epsa.001407.

Gustavo, M., and Gimenez, J. (2021). *Technical regulations for wind Farm integration into power system Part 1: onshore wind power[S]*. Beijing: China Standards Press.

Jiang, M., Guo, Q., Sun, H., and Ge, H. (2021). Short-term voltage stability-constrained unit commitment for receiving-end grid with multi-infeed HVDCs. *IEEE Trans. Power Syst.* 36 (3), 2603–2613. doi:10.1109/tpwrs.2020.3031021

Kuang, L., Wen, Y., Lu, Y., and Lin, X. (2022). Research on frequency stability constrained optimization scheduling model for microgrids with virtual synchronous units. *Proceeding CSEE* 42 (01), 71–83. doi:10.13334/j.0258-8013.pcsee.210127

Li, K., Guo, H., Fang, X., Liu, S., Teng, F., and Chen, Q. (2023a). Market mechanism design of inertia and primary frequency response with consideration of energy market. *IEEE Trans. Power Syst.* 38 (6), 5701–5713. doi:10.1109/tpwrs.2022.3223497

Li, X., Fang, Y., Wu, X., Hou, Y., Li, Z., and Liu, F. (2023b). Quantitative indicators of transient voltage stability based on instability mechanism analysis. *Electr. Power Autom. Equip.* 43 (11), 195–202. doi:10.16081/j.epae.202301023

Lin, Y., Wang, B., Guo, Q., Zhao, H., and Sun, H. (2023b). Short-circuit ratio and short-term voltage security constrained unit commitment in high wind power-injected power systems. *IEEE Trans. Power Syst.* 34 (10), 1–13. doi:10.1109/TPWRS.2023.3347508

Lin, Y., Wang, K., Lai, Y., Chen, H., Zhao, Y., Xu, X., et al. (2023a). Analysis of frequency characteristics of power systems under low inertia and overview of battery energy storage frequency modulation control strategies. *Power grid Technol.* 47 (2), 447–462. doi:10.13335/j.1000-3673.pst.2022.1269

Liu, B., Yang, J., Liao, K., and He, Z. (2016). An improved frequency control scheme for doubly fed wind turbines based on rotor kinetic energy control. *Power Syst. Autom.* 40 (16), 17–22. doi:10.7500/AEPS20150930009

National Energy Administration (2021). *Technical specifications for grid connected operation and control of electrochemical energy storage power plants Part 7 Inertia support and damping control.*

Niu, S., Ke, X., Ren, C., Huo, C., Wang, Z., Zhang, G., et al. (2021). Optimization method for operation mode of large-scale renewable energy DC transmission end power grid based on quantitative evaluation of short-circuit capacity. *Electr. Power Autom. Equip.* 41 (12), 123–129. doi:10.16081/j.epae.202108016

Sun, H., Lin, Y., and Zhao, B. (2023). Quantitative analysis method for voltage support strength of renewable energy grid connected systems based on transient overvoltage constraints. *Proceeding CSEE* 43 (11), 4207–4216. doi:10.13334/j.0258-8013.pcsee.220468

Teng, F., Trovato, V., and Strbac, G. (2016). Stochastic scheduling with inertia-dependent fast frequency response requirements. *IEEE Trans. Power Syst.* 31 (2), 1557–1566. doi:10.1109/tpwrs.2015.2434837

Trovato, V., Bialecki, A., and Dallagi, A. (2019). Unit commitment with inertia-dependent and multispeed allocation of frequency response services. *IEEE Trans. Power Syst.* 34 (2), 1537–1548. doi:10.1109/tpwrs.2018.2870493

Tuo, M., and Li, X. (2023). Security-constrained unit commitment considering locational frequency stability in low-inertia power grids. *IEEE Trans. Power Syst.* 38 (5), 4134–4147. doi:10.1109/tpwrs.2022.3215915

Wang, B., Yang, D., and Cai, G. (2020). Unit commitment considering dynamic frequency constraints under large-scale wind power grid connection conditions. *Power grid Technol.* 44 (7), 2514–2519. doi:10.13335/j.1000-3673.pst.2019.2088

Wang, K., Xie, L., Qiao, Y., Lu, Z., and Yang, H. (2022). Analysis of battery energy storage improving frequency regulation performance of power systems. *Power Syst. autom.* 46 (1), 174–180. doi:10.7500/AEPS20210409002

Wu, L., Li, Y., Yu, S., Sun, Y., Wang, X., Yang, Y., et al. (2022). Stability analysis of wind power collection system based on short-circuit ratio index. *Electr. Power Autom. Equip.* 42 (8), 73–78. doi:10.16081/j.epae.202205030

Xia, Q., Zhong, H., and Kang, C. (2013). Development and prospects of security constrained unit commitment theory and application. *Proceeding CSEE* 33 (16), 94–103.

Xu, X., Ma, S., Huang, Y., and Chang, X. (2015). Large scale wind power integration affects the static voltage stability of the power grid research on impact mechanisms. *China Electr. Power* 48 (3), 139–143.

Xu, Z., Wang, C., Zheng, H., Li, Y., and Han, J. (2020). Unit commitment and economic dispatch of low inertia power grid with energy storage considering frequency constraints. *Adv. Technol. Electr. Eng. Energy* 39 (11), 26–32. doi:10.12067/ATEEE2006038

Xue, Y., Xu, T., Liu, B., and Li, Y. (1999). Transient voltage stability and acceptable voltage drop. *Power Syst. Autom.* 23 (14), 4–8.

Yang, M., Zhang, L., Lyu, J., Xue, B., and Yuan, H. (2020). Flexibility oriented electric energy and auxiliary services Market Joint Clearing Model. *Electr. Power* 53 (8), 182–192. doi:10.11930/j.issn.1004-9649.202006277

Yang, Y., Peng, J.C.-H., Ye, C., Ye, Z. S., and Ding, Y. (2022). A criterion and stochastic unit commitment towards frequency resilience of power systems. *IEEE Trans. Power Syst.* 37 (1), 640–652. doi:10.1109/tpwrs.2021.3095180

Yu, L., Sun, H., Xu, S., Zhao, B., Zhang, J., and Li, Z. (2022a). Overview of quantitative evaluation indicators for voltage support strength of power electronic equipment access. *Proceeding CSEE* 42 (2), 499–514. doi:10.13334/j.0258-8013.pcsee.212126

Yu, L., Sun, H., Zhao, B., Xu, S., Zhang, J., and Li, Z. (2022b). Analysis of short-circuit ratio index and critical short-circuit ratio calculation method for renewable energy grid connected systems. *Proceeding CSEE* 42 (3), 919–928. doi:10.13334/j.0258-8013.pcsee.212399

Zhang, W., Wen, Y., Chi, F., Wang, K., and Li, L. (2021). Research framework and prospects for inertia assessment in power systems. *Proceeding CSEE* 41 (20), 6842–6855. doi:10.13334/j.0258-8013.pcsee.202461

Zhang, Z., Du, E., Teng, F., and Kang, C. (2020). Modeling frequency dynamics in unit commitment with a high share of renewable energy. *IEEE Trans. Power Syst.* 35 (6), 4383–4395. doi:10.1109/tpwrs.2020.2996821

Zheng, L., Hu, W., Lu, Q., Min, Y., Yuan, F., and Gao, Z. (2014). A comprehensive optimization model for planning and operation of energy storage systems for improving wind power access. *Proceeding CSEE* 34 (16), 2533–2543. doi:10.13334/j.0258-8013.pcsee.2014.16.003

Zhongda, C., and Fei, T. (2023). Voltage stability constrained unit commitment in power systems with high penetration of inverter-based generators. *IEEE Trans. Power Syst.* 38 (2), 1572–1582. doi:10.1109/tpwrs.2022.3179563

Zhu, J., Zhu, X., Chen, B., Yu, L., Nie, L., Huang, W., et al. (2024b). New energy inertia time constant evaluation method based on delay compensation. *Power Syst. Autom.* 48 (8), 101–110. doi:10.7500/AEPS20230803006

Zhu, L., Dong, K., Tang, L., Li, Z., and Yu, J. (2024a). A joint optimization and clearing model for electrical energy, inertia, and primary frequency modulation considering the inertia of synchronous unit and virtual inertia of energy storage[J/OL]. *Proceeding CSEE*, 1–14. Available at: http://h-p.kns.cnki.net.shiep.vpn358.com/kcms/detail/11.2107.TM.20230608.1106.003.html.